


 Cite this: *RSC Adv.*, 2022, **12**, 4924

 Received 23rd October 2021  
 Accepted 4th January 2022

DOI: 10.1039/d1ra07835f

[rsc.li/rsc-advances](http://rsc.li/rsc-advances)

# K-doped $\text{Li}_2\text{ZnTi}_3\text{O}_8/\text{C}$ as an efficient anode material with high performance for Li-ion batteries

 Jing Peng,<sup>a</sup> Xianguang Zeng,<sup>b</sup> Huafeng Zhu,<sup>c</sup> Kui Xia<sup>a</sup> and Jing Gong<sup>a</sup>

$\text{Li}_2\text{ZnTi}_3\text{O}_8/\text{C}$  and  $\text{Li}_{1.9}\text{K}_{0.1}\text{ZnTi}_3\text{O}_8/\text{C}$  were successfully synthesized using the sol-gel method. Doping K apparently yielded a wider tunnel, helpful for increasing the rate of transport of lithium ions, and furthermore yielded excellent electrochemical properties. The first discharge capacity for  $\text{Li}_{1.9}\text{K}_{0.1}\text{ZnTi}_3\text{O}_8/\text{C}$  was  $352.9 \text{ mA h g}^{-1}$  at a current density of  $200 \text{ mA g}^{-1}$ .  $\text{Li}_{1.9}\text{K}_{0.1}\text{ZnTi}_3\text{O}_8/\text{C}$  also performed stably, retaining a capacity of  $323.7 \text{ mA h g}^{-1}$  at the 100th cycle, indicative of its excellent cycling properties. In the rate performance test,  $\text{Li}_{1.9}\text{K}_{0.1}\text{ZnTi}_3\text{O}_8/\text{C}$  showed at the first cycle a high discharge capacity of  $379.5 \text{ mA h g}^{-1}$  for a current density of  $50 \text{ mA g}^{-1}$  and a capacity of  $258.9 \text{ mA h g}^{-1}$  at  $1000 \text{ mA g}^{-1}$ . The results indicated that K-doping should be considered a useful method for improving electrochemical performances.

## 1 Introduction

Lithium-ion batteries (LIBs) are effective batteries because of their high specific energy levels, small volumes, long cycling lifetimes and high working voltages,<sup>1–3</sup> and have been used in diverse applications. The anode material, as one of the important components of the LIB, directly affects the electrochemical performance of the battery. Cubic  $\text{Li}_2\text{ZnTi}_3\text{O}_8$  (LZTO) has been investigated as a potential anode material due to its lack of toxicity, high safety, low cost, relatively high theoretical capacity and low discharge voltage plateau of approximately  $0.5 \text{ V}$  (vs.  $\text{Li}/\text{Li}^+$ ).<sup>4–6</sup> But its poor electronic conductivity has restricted its practical applications.<sup>7–10</sup> Therefore, finding methods to improve the electronic and ionic conductivities of LZTO is extremely important.

To overcome such defects, methods such as carbon coating, improving the preparation process, and doping diverse ions have proved effective.<sup>11–22</sup> Carbon materials have great advantages, such as low price, high natural abundance, excellent conductivity, low amounts required for using them to modify other materials, stable physical and chemical properties, *etc.*, which could not only endow the matrix materials with high conductivity, but also reduce the amounts of side reactions between electrode materials and electrolyte. Therefore, carbon inclusion is considered a convenient modification method to improve the electrical conductivity of electrode materials.<sup>20,23,24</sup> Producing small, *i.e.*, nano-sized, particles of lithium ions can

promote the increase of charge-discharge time, and is also conducive to the electrolyte infiltration of the material.<sup>25</sup> The ionic conductivity and electronic conductivity of LZTO can be improved by doping it with ions, and the location and amount of doping affects the electrochemical properties of electrode materials.<sup>11,26–28</sup> The ions currently used for doping lithium zinc titanate mainly include  $\text{Na}^+$ ,  $\text{Ag}^+$ ,<sup>30</sup>  $\text{Al}^{3+}$ ,<sup>31</sup>  $\text{Ce}^{4+}$ ,<sup>10</sup> and  $\text{V}^{5+}$ .<sup>32</sup>

$\text{Na}^+$  is considered a promising doping element due to its high abundance and environmental friendliness. Chen *et al.*<sup>29</sup> has synthesized  $\text{Na}^+$ -doped  $\text{Li}_2\text{ZnTi}_3\text{O}_8$  using the solid state method. Their experiments showed the capacity of  $\text{Li}_{1.95}\text{Na}_{0.05}\text{ZnTi}_3\text{O}_8$  reaching as high as  $267.3 \text{ mA h g}^{-1}$  at the 50th cycle when using a current density of  $0.1 \text{ A g}^{-1}$ . Of the materials they tested, it was shown to display the highest reversible capacity, mainly due to the diameter of  $\text{Na}^+$  being greater than that of  $\text{Li}^+$ , thus enlarging the diffusion channel of  $\text{Li}^+$ .

Tang *et al.*<sup>31</sup> used the solid phase method to add  $\text{Al}_2\text{O}_3$  into  $\text{Li}_2\text{ZnTi}_3\text{O}_8$  to realize the doping with  $\text{Al}^{3+}$ . Their experimental results showed capacity retentions of 99.8%, 91.6%, 86.6% and 93.4% obtained for  $\text{Li}_2\text{ZnTi}_{2.9}\text{Al}_{0.1}\text{O}_8$  at the 100th cycle for current densities of  $0.5 \text{ A g}^{-1}$ ,  $1.0 \text{ A g}^{-1}$ ,  $2.0 \text{ A g}^{-1}$  and  $3.0 \text{ A g}^{-1}$ , respectively. Therefore, the doping of  $\text{Al}^{3+}$  was found to significantly improve the capacity and rate performance of  $\text{Li}_2\text{ZnTi}_3\text{O}_8$ .

Yi *et al.*<sup>32</sup> used  $\text{V}_2\text{O}_5$  as a raw material to synthesize  $\text{V}^{5+}$ -doped  $\text{Li}_2\text{ZnTi}_3\text{O}_8$  by carrying out a simple solid-phase method in one step.  $\text{V}^{5+}$  was found to replace some of the  $\text{Li}^+$  ions and in this way improve the diffusion rate of lithium ions. The reversible capacities of  $\text{Li}_{1.95}\text{V}_{0.05}\text{ZnTi}_3\text{O}_8$  at rates of 0.2, 1.0, 2.0 and  $5.0\text{C}$  were measured to be, respectively, 213.3, 171.2, 132.5 and  $84.7 \text{ mA h g}^{-1}$  values higher than those measured for pure  $\text{Li}_2\text{ZnTi}_3\text{O}_8$  (184.5, 129.5, 107.3 and  $24 \text{ mA h g}^{-1}$ ). Qie *et al.*<sup>33</sup> studied the influence of  $\text{Cu}^{2+}$  doping on the electrochemical

<sup>a</sup>School of Materials Science and Engineering, Sichuan University of Science & Engineering, Zigong 643000, China. E-mail: hnzxg1979@126.com

<sup>b</sup>Material Corrosion and Protection Key Laboratory of Sichuan Province, Zigong 643000, China

<sup>c</sup>Langxingda Technology Co, Ltd., Zigong, 643000, China



properties of  $\text{Li}_2\text{ZnTi}_3\text{O}_8$  and found that  $\text{Li}_{1.95}\text{Zn}_{0.9}\text{Cu}_{0.1}\text{Ti}_3\text{O}_8$  displayed the best electrochemical performance.

K is similar to Li in chemical properties and is a promising doping atom. However, to the best of our knowledge, it has not been used to dope  $\text{Li}_2\text{ZnTi}_3\text{O}_8$ . Therefore, the electrochemical reaction of  $\text{Li}_{1.9}\text{K}_{0.1}\text{ZnTi}_3\text{O}_8/\text{C}$  was studied using the sol-gel method in the current work, and the results showed its excellent electrochemical performance, demonstrating that K-doping should in general be considered a useful method for improving electrochemical performances.

## 2 Materials and methods

$\text{Li}_{1.9}\text{K}_{0.1}\text{ZnTi}_3\text{O}_8/\text{C}$  (0.02 mol) was synthesized using the sol-gel method. To do so, 4.7922 g  $\text{TiO}_2$  (99.8%, Shanghai Maclin Biochemical Technology Co., Ltd), 4.39 g  $(\text{CH}_3\text{COO})_2\text{Zn} \cdot 2\text{H}_2\text{O}$  (AR, Chengdu Cologne Chemical Reagent Co., Ltd), 2.5076 g  $(\text{CH}_3\text{COO})\text{Li}$  (99.9%, Shanghai Maclin Biochemical Technology Co., Ltd), 4 g polyvinylpyrrolidone K30 (PVP K30) (AR, Chengdu Cologne Chemical Reagent Co., Ltd), and 0.1491 g KCl (AR, Chengdu Cologne Chemical Reagent Co., Ltd) were added into a sample of anhydrous ethanol. Then the resulting mixture was dried at 80 °C for 4 h, and the dried material was heated at 750 °C for 15 minutes in a microwave sintering furnace to achieve the final  $\text{Li}_{1.9}\text{K}_{0.1}\text{ZnTi}_3\text{O}_8/\text{C}$  electrode material. For purposes of comparison,  $\text{Li}_2\text{ZnTi}_3\text{O}_8/\text{C}$  was prepared using the same protocol except that KCl was not included.

X-ray diffraction (XRD) patterns were acquired using a Brook AXS's D2 PHASER, with a  $2\theta$  range of 10–80°. Scanning electron

microscopy (SEM) images were acquired using a TESCAN VEGA3 apparatus. X-ray photoelectron spectroscopy (XPS) was carried out using K-K $\alpha$  radiation as the excitation source. Data for high-resolution transmission electron microscopy (HR-TEM) and TEM-EDX mapping were collected using an FEI Talos F200X apparatus. Raman spectra were recorded using a DXR Raman spectrometer (Thermo Scientific) at room temperature with a 780 nm excitation line using an Ar<sup>+</sup> laser.

The electrochemical performance of  $\text{Li}_{1.9}\text{K}_{0.1}\text{ZnTi}_3\text{O}_8/\text{C}$  was assessed with lithium metal as the counter electrode.  $\text{Li}_{1.9}\text{K}_{0.1}\text{ZnTi}_3\text{O}_8/\text{C}$ , Super-P and sodium carboxymethylcellulose (CMC) with a weight ratio of 80 : 10 : 10 were added into water, and the resulting electrode slurry was spread on a copper current collector and dried at 80 °C for 8 h in a vacuum oven. The working electrode was prepared by following the above steps. CR2032 coin cells were prepared in an Ar-filled glovebox. All electrochemical properties were characterized between 0.05 and 3.0 V at 25 °C, and the EIS data were collected at frequencies ranging from 0.1 Hz to 100 kHz.

## 3 Results and discussion

Fig. 1(A) shows the XRD patterns of the materials investigated. All of the samples were determined using these patterns to have formed the spinel LZTO structure, indicating that the low dosage of K<sup>+</sup> did not alter the structure. As shown in Table 1, the cell parameters of  $\text{Li}_2\text{ZnTi}_3\text{O}_8/\text{C}$  and  $\text{Li}_{1.9}\text{K}_{0.1}\text{ZnTi}_3\text{O}_8/\text{C}$  were determined to be, respectively,  $a = 8.4112$  and  $8.5032$  Å with the greater cell length for  $\text{Li}_{1.9}\text{K}_{0.1}\text{ZnTi}_3\text{O}_8/\text{C}$  due to the introduction

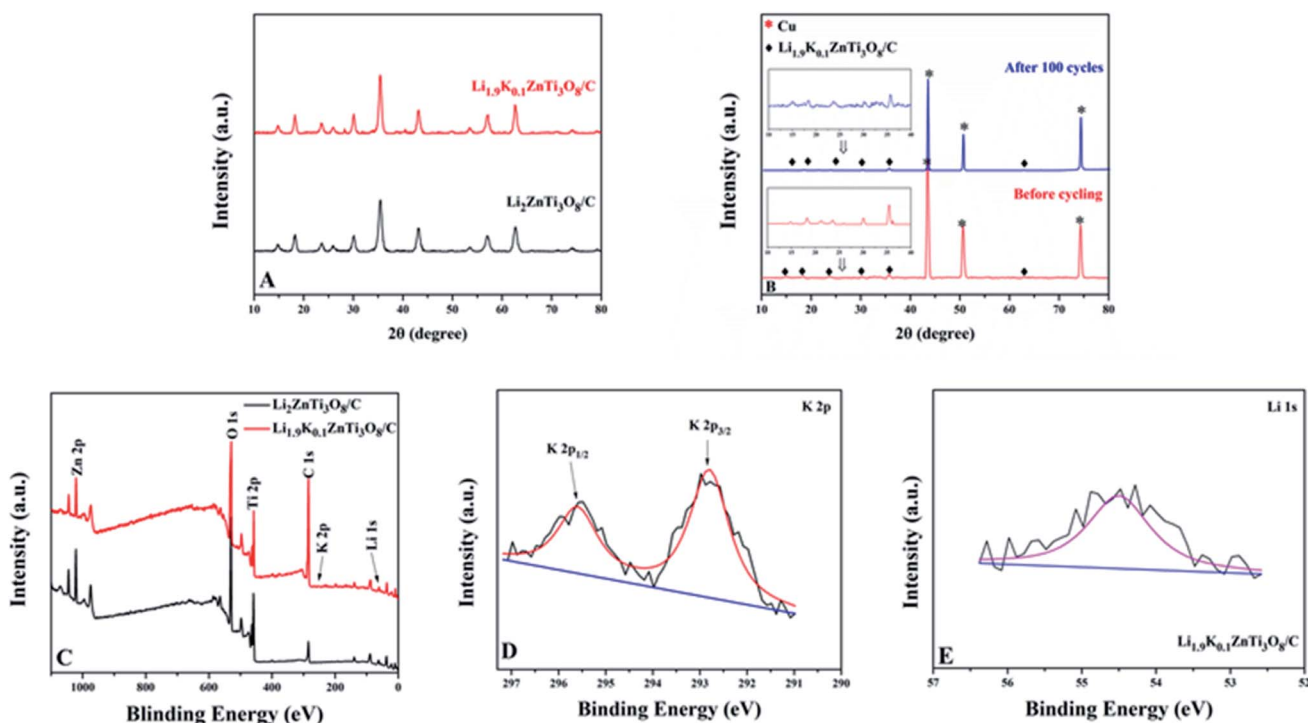


Fig. 1 (A) XRD patterns of  $\text{Li}_2\text{ZnTi}_3\text{O}_8/\text{C}$  and  $\text{Li}_{1.9}\text{K}_{0.1}\text{ZnTi}_3\text{O}_8/\text{C}$ . (B) XRD patterns of  $\text{Li}_{1.9}\text{K}_{0.1}\text{ZnTi}_3\text{O}_8/\text{C}$  before and after 100 cycles. (C) XPS survey spectra of  $\text{Li}_2\text{ZnTi}_3\text{O}_8/\text{C}$  and  $\text{Li}_{1.9}\text{K}_{0.1}\text{ZnTi}_3\text{O}_8/\text{C}$ . (D)  $\text{Li}_{1.9}\text{K}_{0.1}\text{ZnTi}_3\text{O}_8/\text{C}$  XPS spectrum in the K 2p region. (E)  $\text{Li}_2\text{ZnTi}_3\text{O}_8/\text{C}$  and  $\text{Li}_{1.9}\text{K}_{0.1}\text{ZnTi}_3\text{O}_8/\text{C}$  XPS spectra in the Li 1s region.

**Table 1** Crystal lattice parameter values for  $\text{Li}_2\text{ZnTi}_3\text{O}_8/\text{C}$  and  $\text{Li}_{1.9}\text{K}_{0.1}\text{ZnTi}_3\text{O}_8/\text{C}$ 

Samples	Lattice parameters	
	$a$ (Å)	$V$ (Å <sup>3</sup> )
$\text{Li}_{1.9}\text{K}_{0.1}\text{ZnTi}_3\text{O}_8/\text{C}$	8.5032	614.8189
$\text{Li}_2\text{ZnTi}_3\text{O}_8/\text{C}$	8.4112	595.0780

of  $\text{K}^+$  into the crystal structure resulting in a replacement of some of the  $\text{Li}^+$  ions (ionic radius 0.076 Å) with the larger  $\text{K}^+$  ions (ionic radius 1.38 Å).<sup>34,35</sup> This difference was perhaps associated with a wider tunnel for  $\text{Li}_{1.9}\text{K}_{0.1}\text{ZnTi}_3\text{O}_8/\text{C}$ , a feature apt to increase the speed of  $\text{Li}^+$  transport and further improve the electrochemical properties of the resulting electrode material.<sup>36</sup> Fig. 1(B) shows the XRD patterns of  $\text{Li}_{1.9}\text{K}_{0.1}\text{ZnTi}_3\text{O}_8/\text{C}$  before and after 100 cycles. In these patterns, the diffraction peaks were essentially identical, demonstrating that the structure of  $\text{Li}_{1.9}\text{K}_{0.1}\text{ZnTi}_3\text{O}_8/\text{C}$  was very well maintained after 100 cycles.

More information was obtained by taking XPS measurements. Fig. 1(C) shows the XPS survey spectrum of

$\text{Li}_{1.9}\text{K}_{0.1}\text{ZnTi}_3\text{O}_8/\text{C}$ ; peaks corresponding to Li 1s, O 1s, C 1s, Zn 2p, Ti 2p, and K 2p were identified in this spectrum. Peaks observed at about 292.78 and 295.58 eV (Fig. 1(D)) appeared to correspond well to K 2p<sub>3/2</sub> and K 2p<sub>1/2</sub>,<sup>37</sup> verifying the presence of  $\text{K}^+$  in the  $\text{Li}_{1.9}\text{K}_{0.1}\text{ZnTi}_3\text{O}_8/\text{C}$  sample tested. The peak observed at about 54.48 eV in the spectrum of the  $\text{Li}_{1.9}\text{K}_{0.1}\text{ZnTi}_3\text{O}_8/\text{C}$  sample (Fig. 1(E)) can be attributed to Li 1s.<sup>37</sup>

The SEM images (Fig. 2(A) and (B)) acquired of the  $\text{Li}_2\text{ZnTi}_3\text{O}_8/\text{C}$  and  $\text{Li}_{1.9}\text{K}_{0.1}\text{ZnTi}_3\text{O}_8/\text{C}$  samples indicated that they were well crystallized. Note that the particle morphology did not obviously change after the doping with the low dose of  $\text{K}^+$ . More detailed structural information was gained from the TEM images of the  $\text{Li}_2\text{ZnTi}_3\text{O}_8/\text{C}$  and  $\text{Li}_{1.9}\text{K}_{0.1}\text{ZnTi}_3\text{O}_8/\text{C}$  composites (Fig. 2(C) and (D)). And as seen in Fig. 2(E) and (F), no obvious difference between the lattice fringes of these composites was observed, consistent with the XRD results. The results demonstrated that the crystal structure of the composite did not change upon it being doped with small amounts of K. To further investigate the doping into  $\text{Li}_2\text{ZnTi}_3\text{O}_8/\text{C}$ ,  $\text{Li}_{1.9}\text{K}_{0.1}\text{ZnTi}_3\text{O}_8/\text{C}$  was examined using energy dispersive spectroscopy (EDS) mapping. From the EDS mappings, the elements C (Fig. 2(G)),

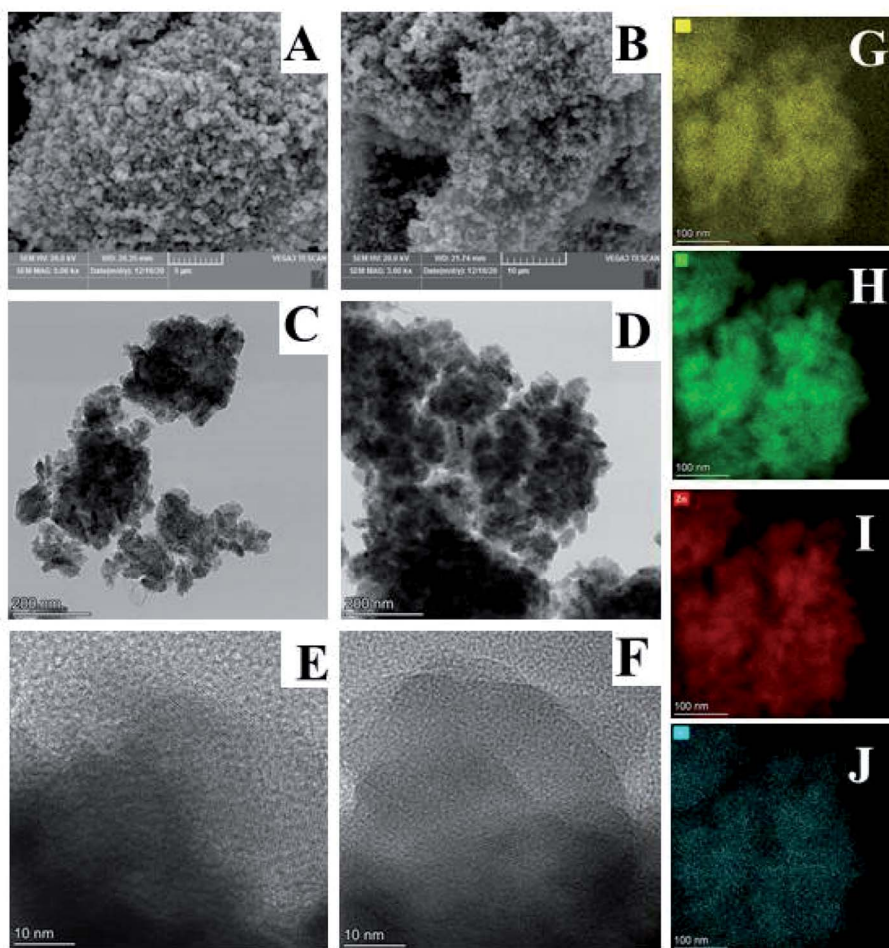


**Fig. 2** (A and B) SEM images of (A)  $\text{Li}_2\text{ZnTi}_3\text{O}_8/\text{C}$  and (B)  $\text{Li}_{1.9}\text{K}_{0.1}\text{ZnTi}_3\text{O}_8/\text{C}$ . (C and D) Typical TEM images of (C)  $\text{Li}_2\text{ZnTi}_3\text{O}_8/\text{C}$  and (D)  $\text{Li}_{1.9}\text{K}_{0.1}\text{ZnTi}_3\text{O}_8/\text{C}$ . (E and F) HRTEM images of (E)  $\text{Li}_2\text{ZnTi}_3\text{O}_8/\text{C}$  and (F)  $\text{Li}_{1.9}\text{K}_{0.1}\text{ZnTi}_3\text{O}_8/\text{C}$ . (G–J) EDS mappings of  $\text{Li}_{1.9}\text{K}_{0.1}\text{ZnTi}_3\text{O}_8/\text{C}$  for the elements (G) C, (H) Ti, (I) Zn, and (J) K.



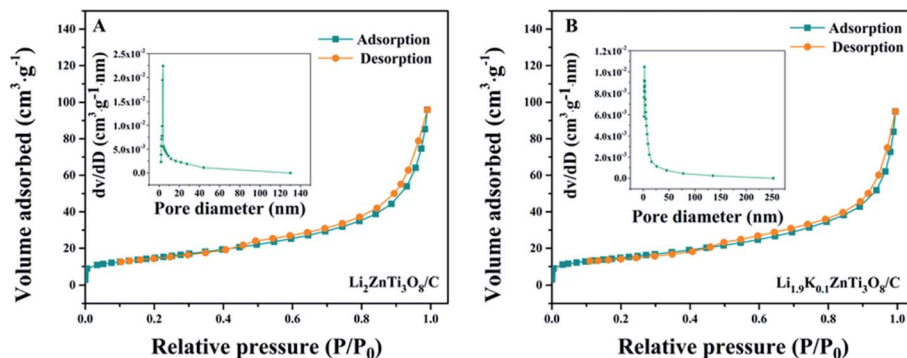


Fig. 3 Nitrogen adsorption–desorption isotherms of (A)  $\text{Li}_2\text{ZnTi}_3\text{O}_8/\text{C}$  and (B)  $\text{Li}_{1.9}\text{K}_{0.1}\text{ZnTi}_3\text{O}_8/\text{C}$  with the corresponding pore diameter distributions in the insets.

Ti (Fig. 2(H)), Zn (Fig. 2(I)) and K (Fig. 2(J)) were seen on the surface of  $\text{Li}_{1.9}\text{K}_{0.1}\text{ZnTi}_3\text{O}_8/\text{C}$ .

The pore size distributions determined using the Barrett–Joyner–Halenda (BJH) method are shown in Fig. 3(A) and (B) (inset). The average diameters of the pores of  $\text{Li}_2\text{ZnTi}_3\text{O}_8/\text{C}$  and  $\text{Li}_{1.9}\text{K}_{0.1}\text{ZnTi}_3\text{O}_8/\text{C}$  were found to be 10.26 nm and 11.13 nm, respectively. From the data obtained, more pores were identified in the  $\text{Li}_{1.9}\text{K}_{0.1}\text{ZnTi}_3\text{O}_8/\text{C}$  material than in the  $\text{Li}_2\text{ZnTi}_3\text{O}_8/\text{C}$  material, which indicated that the degree of agglomeration was reduced and that more tunnels for  $\text{Li}^+$  conduction were provided by  $\text{Li}_{1.9}\text{K}_{0.1}\text{ZnTi}_3\text{O}_8/\text{C}$ .

To verify the presence of carbon in the synthesized  $\text{Li}_2\text{ZnTi}_3\text{O}_8/\text{C}$  and  $\text{Li}_{1.9}\text{K}_{0.1}\text{ZnTi}_3\text{O}_8/\text{C}$  samples, Raman spectra were acquired, as shown in Fig. 4. From the spectra of  $\text{Li}_2\text{ZnTi}_3\text{O}_8/\text{C}$  and  $\text{Li}_{1.9}\text{K}_{0.1}\text{ZnTi}_3\text{O}_8/\text{C}$ , the D band (at *ca.* 1330  $\text{cm}^{-1}$ ) and G band (at *ca.* 1560  $\text{cm}^{-1}$ ) were identified, demonstrating the presence of carbon in the  $\text{Li}_2\text{ZnTi}_3\text{O}_8/\text{C}$  and  $\text{Li}_{1.9}\text{K}_{0.1}\text{ZnTi}_3\text{O}_8/\text{C}$  samples.<sup>38</sup>

The electrochemical reaction mechanisms for  $\text{Li}_2\text{ZnTi}_3\text{O}_8/\text{C}$  and  $\text{Li}_{1.9}\text{K}_{0.1}\text{ZnTi}_3\text{O}_8/\text{C}$  were investigated using cyclic voltammetry (CV). These tests were performed using a scan rate of

0.1  $\text{mV s}^{-1}$  and potentials between 0.05 V and 3 V (Fig. 5 (A) and (B)). The anodic peak potential ( $\varphi_{\text{Pa}}$ ), cathodic peak potential ( $\varphi_{\text{Pc}}$ ) and the difference between them ( $\Delta\varphi_{\text{P}}$ ) are shown in Table 2.  $\text{Li}_2\text{ZnTi}_3\text{O}_8/\text{C}$  and  $\text{Li}_{1.9}\text{K}_{0.1}\text{ZnTi}_3\text{O}_8/\text{C}$  showed cathodic and anodic peaks at potentials between 1 V and 2 V, which we interpreted as involving the participation of the reactions of the  $\text{Ti}^{4+}/\text{Ti}^{3+}$  redox couple, and indicated that applying a low dose of K-doping did not change the  $\text{Li}_2\text{ZnTi}_3\text{O}_8/\text{C}$  electrochemical process.<sup>39</sup> As shown in Table 2, the difference between the potentials of the oxidation and reduction peaks was 151 mV for the  $\text{Li}_2\text{ZnTi}_3\text{O}_8/\text{C}$  sample, but considerably less, at 97 mV, for the  $\text{Li}_{1.9}\text{K}_{0.1}\text{ZnTi}_3\text{O}_8/\text{C}$  sample. Compared with  $\text{Li}_2\text{ZnTi}_3\text{O}_8/\text{C}$ ,  $\text{Li}_{1.9}\text{K}_{0.1}\text{ZnTi}_3\text{O}_8/\text{C}$  has been shown to display higher lithium-ion diffusion rates and lower polarization.<sup>40</sup> Therefore, the reversibility and cycling abilities of the electrode materials were enhanced by the low-dose doping of  $\text{Li}_2\text{ZnTi}_3\text{O}_8/\text{C}$ .

The CV curves for the first cycle at 200  $\text{mA g}^{-1}$  for potentials of 0.05–3 V are shown in Fig. 5(C). Here, the discharge capacity of  $\text{Li}_{1.9}\text{K}_{0.1}\text{ZnTi}_3\text{O}_8/\text{C}$  was higher than that of  $\text{Li}_2\text{ZnTi}_3\text{O}_8/\text{C}$  at the 1st cycle. The voltage of the discharge platform was 0.57 V (vs.  $\text{Li}^+/\text{Li}$ ), the voltage of charging platform was 1.48 V (vs.  $\text{Li}^+/\text{Li}$ ), and the voltage difference between charge and discharge platform was the smallest, indicating that the polarization of the synthesized material was small during  $\text{Li}^+$  disintercalation.<sup>41</sup>

The cycling properties of  $\text{Li}_2\text{ZnTi}_3\text{O}_8/\text{C}$  and  $\text{Li}_{1.9}\text{K}_{0.1}\text{ZnTi}_3\text{O}_8/\text{C}$  were characterized at 200  $\text{mA g}^{-1}$  (Fig. 5(D)). At the 100th cycle, 75.06% and 91.73% (323.7  $\text{mA h g}^{-1}$ ) of the initial capacities were retained for  $\text{Li}_2\text{ZnTi}_3\text{O}_8/\text{C}$  and  $\text{Li}_{1.9}\text{K}_{0.1}\text{ZnTi}_3\text{O}_8/\text{C}$ , respectively. Chen *et al.*<sup>29</sup> synthesized  $\text{Li}_{1.95}\text{Na}_{0.05}\text{ZnTi}_3\text{O}_8$ , and it reached 267.3  $\text{mA h g}^{-1}$  at the 50th cycle at 0.1  $\text{A g}^{-1}$ , indicating a better cycling performance resulting from  $\text{K}^+$  doping than from  $\text{Na}^+$  doping. Therefore,  $\text{Li}_{1.9}\text{K}_{0.1}\text{ZnTi}_3\text{O}_8/\text{C}$  was indicated to demonstrate a better capacity retention and cycling performance than  $\text{Li}_2\text{ZnTi}_3\text{O}_8/\text{C}$ , which could be attributed to the low-dose  $\text{K}^+$  doping enlarging the  $\text{Li}^+$  transport tunnels, and hence increasing the rates of  $\text{Li}^+$  transport and electron transport.<sup>36</sup>

The rate properties of  $\text{Li}_2\text{ZnTi}_3\text{O}_8/\text{C}$  and  $\text{Li}_{1.9}\text{K}_{0.1}\text{ZnTi}_3\text{O}_8/\text{C}$  are compared in Fig. 5(E).  $\text{Li}_{1.9}\text{K}_{0.1}\text{ZnTi}_3\text{O}_8/\text{C}$  delivered a maximum discharge capacity of 379.5  $\text{mA h g}^{-1}$  at the 1st cycle for a current density of 50  $\text{mA g}^{-1}$ , and discharge capacities of

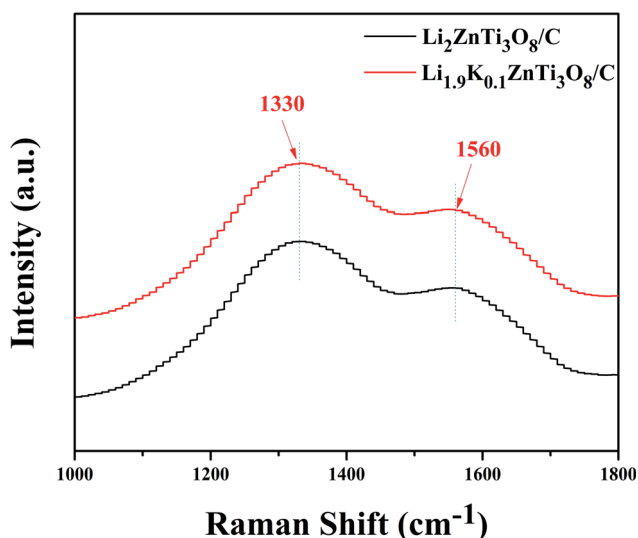


Fig. 4 Raman spectra of  $\text{Li}_2\text{ZnTi}_3\text{O}_8/\text{C}$  and  $\text{Li}_{1.9}\text{K}_{0.1}\text{ZnTi}_3\text{O}_8/\text{C}$ .



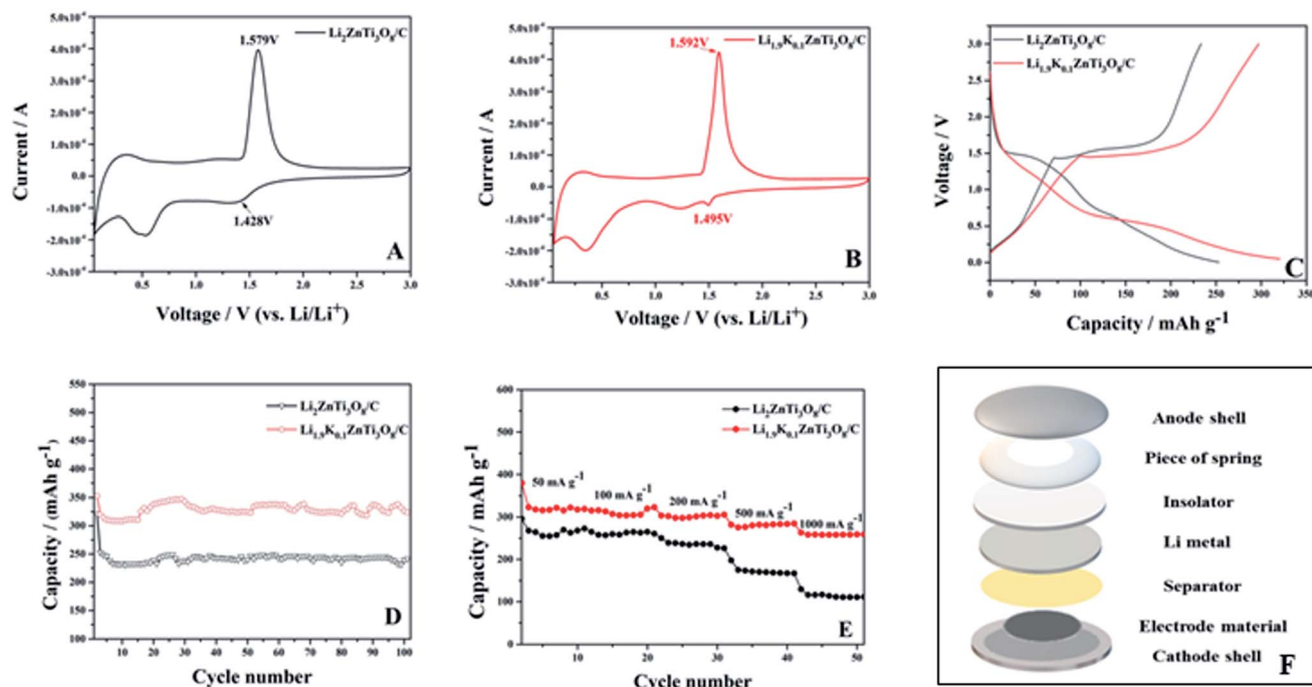


Fig. 5 (A and B) CV curves of (A)  $\text{Li}_2\text{ZnTi}_3\text{O}_8/\text{C}$  and (B)  $\text{Li}_{1.9}\text{K}_{0.1}\text{ZnTi}_3\text{O}_8/\text{C}$  from 0.05 V to 3.0 V. (C) Initial charge–discharge curves of  $\text{Li}_2\text{ZnTi}_3\text{O}_8/\text{C}$  and  $\text{Li}_{1.9}\text{K}_{0.1}\text{ZnTi}_3\text{O}_8/\text{C}$ . (D) Cycling capacity of  $\text{Li}_2\text{ZnTi}_3\text{O}_8/\text{C}$  and  $\text{Li}_{1.9}\text{K}_{0.1}\text{ZnTi}_3\text{O}_8/\text{C}$  for 100 cycles. (E) Rate performances of  $\text{Li}_2\text{ZnTi}_3\text{O}_8/\text{C}$  and  $\text{Li}_{1.9}\text{K}_{0.1}\text{ZnTi}_3\text{O}_8/\text{C}$  at different current densities. (F) The composition of the CR2032 button battery.

Table 2 Electrochemical parameters of investigated samples, including the difference between the potentials of the anodic and cathodic peaks from CV

Sample	$\varphi_{\text{Pa}}$ (V)	$\varphi_{\text{Pc}}$ (V)	$\Delta\varphi_{\text{P}}$ (mV)
$\text{Li}_{1.9}\text{K}_{0.1}\text{ZnTi}_3\text{O}_8/\text{C}$	1.592	1.495	97
$\text{Li}_2\text{ZnTi}_3\text{O}_8/\text{C}$	1.579	1.428	151

322.9, 305.5, 284.5, and 258.9  $\text{mA h g}^{-1}$  for 100, 200, 500, and 1000  $\text{mA g}^{-1}$ , respectively, whereas  $\text{Li}_2\text{ZnTi}_3\text{O}_8/\text{C}$  delivered capacities of 260.6, 226.2, 166.9, and 111.4  $\text{mA h g}^{-1}$  at these current densities, respectively.  $\text{Li}_{1.9}\text{K}_{0.1}\text{ZnTi}_3\text{O}_8/\text{C}$  showed better rate properties than did  $\text{Li}_2\text{ZnTi}_3\text{O}_8/\text{C}$ , which may be attributed to (1) doping K possibly having enhanced the electronic conductivity and yielding a good rate performance for  $\text{Li}_{1.9}\text{K}_{0.1}\text{ZnTi}_3\text{O}_8/\text{C}$ , and (2) the increased cell volume after low-dose K doping possibly increasing the rates of  $\text{Li}^+$  transport and electron transport.<sup>42,43</sup>

EIS measurements for the samples were taken as shown in Fig. 6. The corresponding plots were composed of a semicircle at high frequency and an inclined line at the low-frequency region, indicating the charge transfer resistance and  $\text{Li}^+$  diffusion process within the electrodes, respectively.<sup>44,45</sup> As shown in Fig. 6, the charge-transfer resistance of the  $\text{Li}_{1.9}\text{K}_{0.1}\text{ZnTi}_3\text{O}_8/\text{C}$  was found to be lower than that of  $\text{Li}_2\text{ZnTi}_3\text{O}_8/\text{C}$ , demonstrating low-dose  $\text{K}^+$  doping to be a useful method for enhancing the electronic conductivity.<sup>46,47</sup> In addition, according to the data in

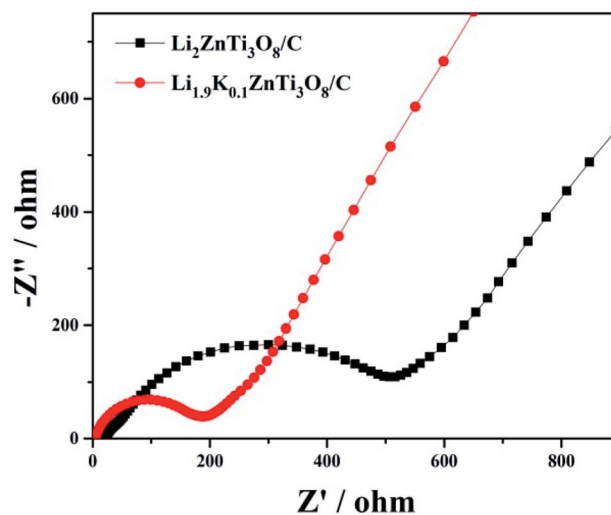


Fig. 6 EIS results for  $\text{Li}_2\text{ZnTi}_3\text{O}_8/\text{C}$  and  $\text{Li}_{1.9}\text{K}_{0.1}\text{ZnTi}_3\text{O}_8/\text{C}$ .

the low-frequency regions, the  $\text{Li}^+$  diffusion rate of the  $\text{Li}_{1.9}\text{K}_{0.1}\text{ZnTi}_3\text{O}_8/\text{C}$  sample was slightly higher than that of the  $\text{Li}_2\text{ZnTi}_3\text{O}_8/\text{C}$  sample.

## 4 Conclusions

In this study, an XRD analysis indicated no change in the structure of  $\text{Li}_2\text{ZnTi}_3\text{O}_8/\text{C}$  resulting from introducing into it a low dose of K. In addition, a low dose of K doped into



$\text{Li}_2\text{ZnTi}_3\text{O}_8/\text{C}$  was good for enhancing the electronic and ionic conductivity levels, which could improve the electrochemical performance. The initial discharge capacity was  $352.9 \text{ mA h g}^{-1}$  ( $\text{Li}_{1.9}\text{K}_{0.1}\text{ZnTi}_3\text{O}_8/\text{C}$ ) at  $200 \text{ mA g}^{-1}$ . The sample performed stably, with a capacity of  $323.7 \text{ mA h g}^{-1}$  retained for  $\text{Li}_{1.9}\text{K}_{0.1}\text{ZnTi}_3\text{O}_8/\text{C}$  after 100 cycles. In the rate test,  $\text{Li}_{1.9}\text{K}_{0.1}\text{ZnTi}_3\text{O}_8/\text{C}$  showed a high discharge capacity of  $379.5 \text{ mA h g}^{-1}$  at the 1st cycle for a current density of  $50 \text{ mA g}^{-1}$  and a capacity of  $258.9 \text{ mA h g}^{-1}$  for  $1000 \text{ mA g}^{-1}$ . Of the various materials tested,  $\text{Li}_{1.9}\text{K}_{0.1}\text{ZnTi}_3\text{O}_8/\text{C}$  exhibited the best rate properties and excellent cycling stability. Therefore, K-doping should be considered a useful method for improving electrochemical performances.

## Funding

This work was financially supported by the Demonstration Project of Scientific and Technological Achievements Transfer and Transformation of Sichuan Province (2021ZHCG0040).

## Author contributions

X.-G. Zeng and J. Peng contributed to the conception and design of the study. H.-F. Zhu and K. Xia organized the database. J. Peng and J. Gong wrote the first draft of the manuscript. X.-G. Zeng revised the whole manuscript.

## Conflicts of interest

The authors declare that the research was conducted in the absence of any commercial or financial relationships that could be construed as a potential conflict of interest.

## References

- 1 T. Liu, H. Tang, J. Liu, *et al.*, Improved electrochemical performance of  $\text{Li}_2\text{ZnTi}_3\text{O}_8$  using carbon materials as loose and porous agent, *Electrochim. Acta*, 2018, **259**, 28–35.
- 2 T. Liu, H. Tang, L. Zan, *et al.*, Comparative study of  $\text{Li}_2\text{ZnTi}_3\text{O}_8$  anode material with good high rate capacities prepared by solid state, molten salt and sol-gel methods, *J. Electroanal. Chem.*, 2016, **771**, 10–16.
- 3 G. Li, X. Chen, Y. F. Liu, *et al.*, One-time sintering process to synthesize  $\text{ZrO}_2$ -coated  $\text{LiMn}_2\text{O}_4$  materials for lithium-ion batteries, *RSC Adv.*, 2018, **8**, 16753–16761.
- 4 C. An, C. Li, H. Tang, *et al.*, Binder-free flexible  $\text{Li}_2\text{ZnTi}_3\text{O}_8$ @MWCNTs stereoscopic network as lightweight and superior rate performance anode for lithium-ion batteries, *J. Alloys Compd.*, 2020, **816**, 152580.
- 5 C. Chen, Z. Li and B. Xu, Surface modification of  $\text{Li}_2\text{ZnTi}_3\text{O}_8$  with the C&N layer for lithium-ion batteries, *Mater. Chem. Phys.*, 2020, **245**.
- 6 N. Firdous, N. Arshad, S. B. Simonsen, *et al.*, Advanced electrochemical investigations of niobium modified  $\text{Li}_2\text{ZnTi}_3\text{O}_8$  lithium ion battery anode materials, *J. Power Sources*, 2020, **462**, 228186.
- 7 C. Chen, C. Ai, Y. He, *et al.*, High performance  $\text{Li}_2\text{ZnTi}_3\text{O}_8$  coated with N-doped carbon as an anode material for lithium-ion batteries, *J. Alloys Compd.*, 2017, **705**, 438–444.
- 8 C. Chen, C. Ai and X. Liu, Ti(III) self-doped  $\text{Li}_2\text{ZnTi}_3\text{O}_8$  as a superior anode material for Li-ion batteries, *Electrochim. Acta*, 2018, **265**, 448–454.
- 9 C. Chen, C. Ai, X. Liu, *et al.*, High performance  $\text{Li}_2\text{ZnTi}_3\text{O}_8$ @C anode material fabricated by a facile method without an additional carbon source, *J. Alloys Compd.*, 2017, **698**, 692–698.
- 10 C. Chen, C. Ai, X. Liu, *et al.*, Advanced electrochemical properties of Ce-modified  $\text{Li}_2\text{ZnTi}_3\text{O}_8$  anode material for lithium-ion batteries, *Electrochim. Acta*, 2017, **227**, 285–293.
- 11 Y. J. Bai, C. Gong, Y. X. Qi, *et al.*, Excellent long-term cycling stability of La-doped  $\text{Li}_4\text{Ti}_5\text{O}_{12}$  anode material at high current rates, *J. Mater. Chem.*, 2012, **22**, 19054.
- 12 Y. R. Jhan and J. G. Duh, Electrochemical performance and low discharge cut-off voltage behavior of ruthenium doped  $\text{Li}_4\text{Ti}_5\text{O}_{12}$  with improved energy density, *Electrochim. Acta*, 2012, **63**, 9–15.
- 13 C. Y. Lin, Y. R. Jhan and J. G. Duh, Improved capacity and rate capability of Ru-doped and carbon-coated  $\text{Li}_4\text{Ti}_5\text{O}_{12}$  anode material, *J. Alloys Compd.*, 2011, **509**, 6965–6968.
- 14 V. Mani, K. Nathiya and N. Kalaiselvi, Role of carbon content in qualifying  $\text{Li}_3\text{V}_2(\text{PO}_4)_3/\text{C}$  as a high capacity anode for high rate lithium battery applications, *RSC Adv.*, 2014, **4**, 17091–17096.
- 15 Y. Qi, Y. Huang, D. Jia, *et al.*, Preparation and characterization of novel spinel  $\text{Li}_4\text{Ti}_5\text{O}_{12-x}\text{Br}_x$  anode materials, *Electrochim. Acta*, 2009, **54**, 4772–4776.
- 16 A. Y. Shenouda and K. R. Murali, Electrochemical properties of doped lithium titanate compounds and their performance in lithium rechargeable batteries, *J. Power Sources*, 2008, **176**, 332–339.
- 17 B. Tian, H. Xiang, L. Zhang, *et al.*, Niobium doped lithium titanate as a high rate anode material for Li-ion batteries, *Electrochim. Acta*, 2010, **55**, 5453–5458.
- 18 S. Wang, L. Wang, Z. Meng, *et al.*,  $\text{Li}_2\text{ZnTi}_3\text{O}_8$ /graphene nanocomposite as a high-performance anode material for lithium-ion batteries, *RSC Adv.*, 2018, **8**, 31628–31632.
- 19 H. Wu, S. Chang, X. Liu, *et al.*, Sr-doped  $\text{Li}_4\text{Ti}_5\text{O}_{12}$  as the anode material for lithium-ion batteries, *Solid State Ionics*, 2013, **232**, 13–18.
- 20 Y. Xu, Z. Hong, L. Xia, *et al.*, One step sol-gel synthesis of  $\text{Li}_2\text{ZnTi}_3\text{O}_8/\text{C}$  nanocomposite with enhanced lithium-ion storage properties, *Electrochim. Acta*, 2013, **88**, 74–78.
- 21 Z. Yu, X. Zhang, G. Yang, *et al.*, High rate capability and long-term cyclability of  $\text{Li}_4\text{Ti}_4.9\text{V}_{0.1}\text{O}_{12}$  as anode material in lithium ion battery, *Electrochim. Acta*, 2011, **56**, 8611–8617.
- 22 B. Zhang, Z. D. Huang, S. W. Oh, *et al.*, Improved rate capability of carbon coated  $\text{Li}_{3.9}\text{Sn}_{0.1}\text{Ti}_5\text{O}_{12}$  porous electrodes for Li-ion batteries, *J. Power Sources*, 2011, **196**, 10692–10697.
- 23 H. Tang and Z. Tang, Effect of different carbon sources on electrochemical properties of  $\text{Li}_2\text{ZnTi}_3\text{O}_8/\text{C}$  anode material in lithium-ion batteries, *J. Alloys Compd.*, 2014, **613**, 267–274.



- 24 L. Zeng, C. Zheng, L. Xia, *et al.*, Ordered mesoporous TiO<sub>2</sub>-C nanocomposite as an anode material for long-term performance lithium-ion batteries, *J. Mater. Chem. A*, 2013, **1**, 4293.
- 25 L. Wang, L. Wu, Z. Li, *et al.*, Synthesis and electrochemical properties of Li<sub>2</sub>ZnTi<sub>3</sub>O<sub>8</sub> fibers as an anode material for lithium-ion batteries, *Electrochim. Acta*, 2011, **56**, 5343–5346.
- 26 W. Fang, X. Cheng, P. Zuo, *et al.*, A facile strategy to prepare nano-crystalline Li<sub>4</sub>Ti<sub>5</sub>O<sub>12</sub>/C anode material *via* polyvinyl alcohol as carbon source for high-rate rechargeable Li-ion batteries, *Electrochim. Acta*, 2013, **93**, 173–178.
- 27 Y. Li, L. Wang, K. Zhang, *et al.*, An encapsulation of phosphorus doped carbon over LiFePO<sub>4</sub> prepared under vacuum condition for lithium-ion batteries, *Vacuum*, 2021, 184.
- 28 C. Lin, M. O. Lai, H. Zhou, *et al.*, Mesoporous Li<sub>4</sub>Ti<sub>5</sub>O<sub>(12-x)</sub>/C submicrospheres with comprehensively improved electrochemical performances for high-power lithium-ion batteries, *Phys. Chem. Chem. Phys.*, 2014, **16**, 24874–24883.
- 29 W. Chen, Z. Zhou, R. Wang, *et al.*, High performance Na-doped lithium zinc titanate as anode material for Li-ion batteries, *RSC Adv.*, 2015, **5**, 49890–49898.
- 30 H. Tang, Z. Tang, C. Du, *et al.*, Ag-doped Li<sub>2</sub>ZnTi<sub>3</sub>O<sub>8</sub> as a high rate anode material for rechargeable lithium-ion batteries, *Electrochim. Acta*, 2014, **120**, 187–192.
- 31 H. Tang, J. Zhu, Z. Tang, *et al.*, Al-doped Li<sub>2</sub>ZnTi<sub>3</sub>O<sub>8</sub> as an effective anode material for lithium-ion batteries with good rate capabilities, *J. Electroanal. Chem.*, 2014, **731**, 60–66.
- 32 T. F. Yi, J. Z. Wu, J. Yuan, *et al.*, Rapid Lithiation and Delithiation Property of V-Doped Li<sub>2</sub>ZnTi<sub>3</sub>O<sub>8</sub> as Anode Material for Lithium-Ion Battery, *ACS Sustainable Chem. Eng.*, 2015, **3**, 3062–3069.
- 33 F. Qie and Z. Tang, Cu-doped Li<sub>2</sub>ZnTi<sub>3</sub>O<sub>8</sub> anode material with improved electrochemical performance for lithium-ion batteries, *Mater. Express*, 2014, **4**, 221–227.
- 34 Z. Zhang, R. Xun, L. Wang, *et al.*, Construction of pseudocapacitive Li<sub>2-x</sub>La<sub>x</sub>ZnTi<sub>3</sub>O<sub>8</sub> anode for fast and super-stable lithium storage, *Ceram. Int.*, 2021, **47**, 662–669.
- 35 Z. Liu, Z. Zhang, Y. Liu, *et al.*, Facile and scalable fabrication of K<sup>+</sup>-doped Li<sub>1.2</sub>Ni<sub>0.2</sub>Co<sub>0.08</sub>Mn<sub>0.52</sub>O<sub>2</sub> cathode with ultra high capacity and enhanced cycling stability for lithium ion batteries, *Solid State Ionics*, 2019, **332**, 47–54.
- 36 Z. Tai, W. Zhu, M. Shi, *et al.*, Improving electrochemical performances of Lithium-rich oxide by cooperatively doping Cr and coating Li<sub>3</sub>PO<sub>4</sub> as cathode material for Lithium-ion batteries, *J. Colloid Interface Sci.*, 2020, **576**, 468–475.
- 37 H. Yang, X. H. Wang, Y. X. Qi, *et al.*, Improving the Electrochemical Performance of Li<sub>2</sub>ZnTi<sub>3</sub>O<sub>8</sub> by Surface KCl Modification, *ACS Sustainable Chem. Eng.*, 2017, **5**, 6099–6106.
- 38 J. L. Qin, H. L. Zhu, N. Lun, *et al.*, Li<sub>2</sub>ZnTi<sub>3</sub>O<sub>8</sub>/C anode with high initial Coulombic efficiency, long cyclic life and outstanding rate properties enabled by fulvic acid, *Carbon*, 2020, **163**, 297–307.
- 39 W. Chen, H. Liang, L. Shao, *et al.*, Observation of the structural changes of sol-gel formed Li<sub>2</sub>MnTi<sub>3</sub>O<sub>8</sub> during electrochemical reaction by *in situ* and *ex situ* studies, *Electrochim. Acta*, 2015, **152**, 187–194.
- 40 S. Wang, Y. Bi, L. Wang, *et al.*, Mo-doped Li<sub>2</sub>ZnTi<sub>3</sub>O<sub>8</sub>@graphene as a high performance anode material for lithium-ion batteries, *Electrochim. Acta*, 2019, **301**, 319–324.
- 41 P. Zhang, X. Li, Y. Hua, *et al.*, Enhanced performance and anchoring polysulfide mechanism of carbon aerogel/sulfur material with Cr doping and pore tuning for Li-S batteries, *Electrochim. Acta*, 2018, **282**, 499–509.
- 42 Y. Nie, W. Xiao, C. Miao, *et al.*, Boosting the electrochemical performance of LiNi<sub>0.8</sub>Co<sub>0.15</sub>Al<sub>0.05</sub>O<sub>2</sub> cathode materials *in situ* modified with Li<sub>1.3</sub>Al<sub>0.3</sub>Ti<sub>1.7</sub>(PO<sub>4</sub>)<sub>3</sub> fast ion conductor for lithium-ion batteries, *Electrochim. Acta*, 2020, 353.
- 43 Y. Chen, Y. Zhao, X. An, *et al.*, Preparation and electrochemical performance studies on Cr-doped Li<sub>3</sub>V<sub>2</sub>(PO<sub>4</sub>)<sub>3</sub> as cathode materials for lithium-ion batteries, *Electrochim. Acta*, 2009, **54**, 5844–5850.
- 44 Y. Q. Tang, X. Liu, X. B. Huang, *et al.*, Synthesis and electrochemical properties of Li<sub>2</sub>FeSiO<sub>4</sub>/C/Ag composite as a cathode material for Li-ion battery, *J. Cent. South Univ.*, 2019, **26**, 1443–1448.
- 45 W. Long, X. Wang, S. Yang, *et al.*, Electrochemical properties of Li<sub>4</sub>Ti<sub>5-2x</sub>Ni<sub>x</sub>Mn<sub>x</sub>O<sub>12</sub> compounds synthesized by sol-gel process, *Mater. Chem. Phys.*, 2011, **131**, 431–435.
- 46 Z. Li, Y. Cui, J. Wu, *et al.*, Synthesis and electrochemical properties of lithium zinc titanate as an anode material for lithium ion batteries *via* microwave method, *RSC Adv.*, 2016, **6**, 39209–39215.
- 47 Z. Kou, C. Miao, P. Mei, *et al.*, Enhancing the cycling stability of all-solid-state lithium-ion batteries assembled with Li<sub>1.3</sub>Al<sub>0.3</sub>Ti<sub>1.7</sub>(PO<sub>4</sub>)<sub>3</sub> solid electrolytes prepared from precursor solutions with appropriate pH values, *Ceram. Int.*, 2020, **46**, 9629–9636.

